ACS Catalysis

pubs.acs.org/acscatalysis Research Article

Imaging Reactivity of the Pt−Ionomer Interface in Fuel-Cell Catalyst Layers

Isaac Martens,* Lis G. A. Melo, Marcia M. West, David P. Wilkinson, Dan Bizzotto, and Adam P. Hitchcock

Cite This: *ACS Catal.* 2020, 10, 8285−8292 Read Online

ACCESS | Metrics & More | Article Recommendations | Supporting Information

ABSTRACT: The interface between perfluorosulfonic acid polymer electrolytes and Pt nanoparticles in a model hydrogen fuel-cell catalyst layer was analyzed using high-resolution scanning transmission X-ray microscopy. After electrochemical cycling, thin films of damaged ionomer, enriched in C═C bonds, are observed near the Pt surface. This local degradation of the Pt−ionomer interface triggered by electrochemical oxidation contrasts with that from peroxide radical exposure. Peroxide damage is catalyzed by Pt and leads instead to thin films containing carboxylic acids. Direct mapping of the degradation at these nanoscale interfaces inside hydrogen fuel-cell catalyst layers exposes a previously unknown electrochemical reactivity of perfluorinated ionomers.

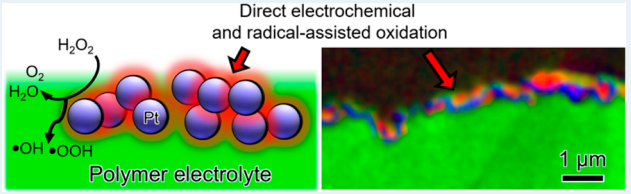

KEYWORDS: *ionomer, STXM, fuel cell, electrocatalysis, Nafion, catalyst layer, polymer electrolyte*

INTRODUCTION

The durability of polymer electrolyte membrane fuel-cell (PEMFC) systems is presently a limiting factor in their commercial adoption.[1−3] These devices exhibit complex, composite interfaces which directly influence performance.[4−6] A better understanding of their structure and the mechanisms of aging and degradation phenomena will be critical in designing next-generation systems.[7,8]

The blended nanocomposite interface found inside PEMFC catalyst layers makes detailed structural analysis very complicated, even by advanced characterization techniques.[9−12] Conventional catalyst layers consist of a Pt/C catalyst, perfluorosulfonic acid (PFSA) polymer electrolyte (e.g., Nafion), and carbon support which are dispersed into an ink and spray painted into a porous film. The resulting 3D morphology is challenging to analyze. Despite the active development of several sophisticated techniques, the fate of each component in the film cannot be easily isolated, especially at the scale of catalyst particles and particle agglomerates.[13−15] Better control over the specific interactions between polymer electrolytes and catalysts is increasingly necessary for the optimization and advancement of catalyst layer architectures.[16−18]

The stability of the Pt/ionomer interface contributes not only to the total lifetime of the catalyst layer but also to the cell performance. Poor control over ink formulation and film deposition can lead to the ionomer poisoning the catalyst surface, blocking oxygen reduction.[19,20] Corrosion and segregation of the ionomer induced by electrochemical cycling can disrupt the local proton conductivity and increase cell resistance, further decreasing the catalyst activity over time.[7]

The potential-dependent structure of the Pt/ionomer interface has been measured numerous times using high-quality electrochemistry and spectroelectrochemical measurements on well-defined and nanoparticle surfaces.[21−28] However, the stability of the PFSA surrounding these interfaces remains poorly understood.[29,30] Vibrational spectromicroscopy indicates that ionomer degradation is spatially correlated with Pt inside membranes, but that technique has poor resolution and is complicated by the chemical gradients inside cells.[31] The structural evolution of the interface with respect to potential cycling and its link to cell performance have not been thoroughly examined.

The interactions between PFSA and the Pt surface were studied using a model catalyst layer of electrolessly deposited Pt grown on/into the surface of a PFSA membrane, as reported previously.[32] This architecture creates a reasonably well-defined, high surface area interface between the Pt catalyst and the PFSA. Relative to planar electrodes, the small Pt nanoparticles (3−10 nm) have a large electrochemical surface area (~20 m^2/g). This approach has two key advantages. First, the catalyst is free of graphitic carbon support, which allows for the carbon K-edge spectroscopy of the PFSA to be probed free from interference. Second, the resulting film can be thin

Received: April 8, 2020
Revised: June 30, 2020
Published: July 1, 2020

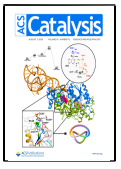

https://dx.doi.org/10.1021/acscatal.0c01594
ACS Catal. 2020, 10, 8285−8292

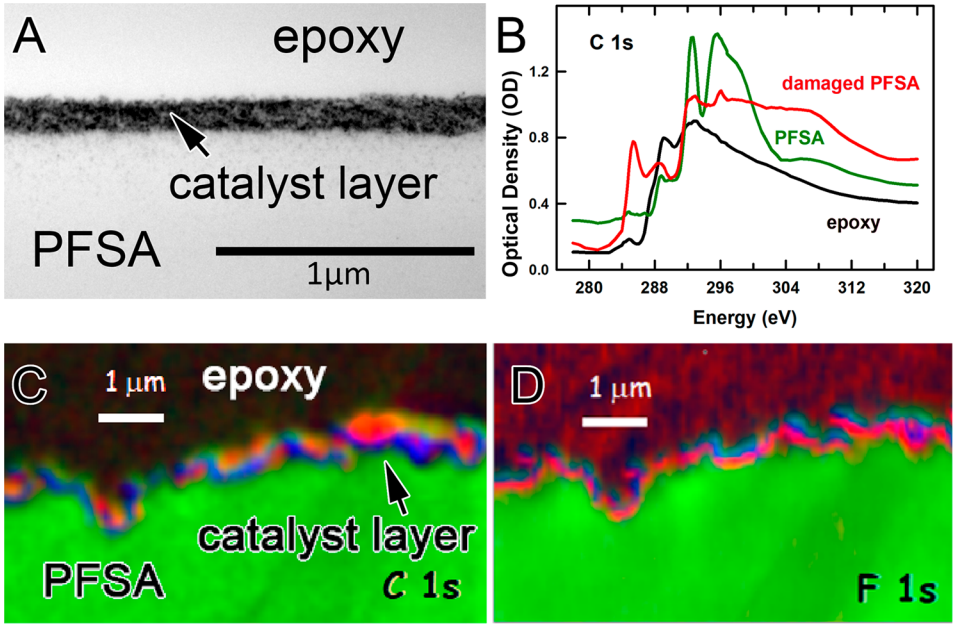

Figure 1. Bright-field TEM cross-section image of initial Pt catalyst thin film after deposition on an ionomer membrane before electrochemical aging (A). STXM cross-section image of the catalyst layer after electrochemical aging up to 1.5 V. Color-coded chemical maps of undamaged PFSA (green), electrochemically damaged PFSA (red), and Pt (blue) derived from fits to (C) C 1s and (D) F 1s image sequences (stacks) of the cycled catalyst layer recorded by STXM. (B) C 1s X-ray spectra extracted from the C 1s stack of the region shown in C.

sectioned using ultramicrotomy, allowing high-resolution cross-sectional analysis.[33,34]

In this study, we show how X-ray spectromicroscopy can be used to probe the chemical and electrochemical reactivity of the Pt−ionomer interface. Spatially resolved X-ray absorption spectroscopy measured in the X-ray microscope reveals that Nafion in contact with Pt is degraded under conditions found inside fuel cells. Prior assumptions about the inert nature of this interface may need to be revisited in light of the central importance of that interface to device operation.

EXPERIMENTAL METHODS

The fabrication and electrochemical characterization of the electrolessly deposited catalyst layer was performed as previously described.[32] X-ray microscopy was performed at the 10ID1 beamline at the Canadian Light Source and the 5.3.3.2 beamline at the Advanced Light Source. Detailed procedures for the X-ray, electron, infrared, and atomic force microscopies can be found in the Supporting Information.

The STXM chemical maps were obtained by recording sequences of X-ray microscopy images at 50−100 photon energies at each of the C 1s and F 1s edges. First, the image sequences (stacks) were aligned and converted to optical density (OD). Spectra were extracted from suitable regions and used as references for a singular value decomposition (SVD) of each image stack into spatial distribution maps of each component. The Pt catalyst was fit by a constant. Three components (PFSA, modified PFSA, and embedding epoxy) plus a constant were used to fit the C 1s stacks. Two components and a constant were used to fit F 1s maps. Regions far from the Pt interface (near the top and bottom of the images) were used as reference spectra of bulk unmodified PFSA and the epoxy to guide the analysis. A detailed discussion of analysis procedures for STXM studies of PEMFC materials has been published elsewhere.[35]

RESULTS AND DISCUSSION

Electrochemical Reactivity of PFSA. The catalyst layer was sandwiched against a carbon fiber paper to make conductive contact and electrochemically characterized in a half-cell. The catalyst film was subjected to an accelerated stress test using cyclic voltammetry, simulating the potentials experienced inside a fuel-cell cathode during startup and shutdown (5000 cycles between 1.0 and 1.5 V vs RHE, 500 mV/s).[36] This protocol is commonly used to assess the stability of the carbon black catalyst support particles, which corrode under these conditions.[35] The resulting catalyst layer was delaminated, cut into ultrathin sections, and imaged using scanning transmission X-ray microscopy (STXM). Detailed protocols for this analysis have been published elsewhere.[37]

Low-magnification transmission electron microscopy (TEM) imaging of the catalyst layer cross section after deposition shows the expected thin film of Pt embedded in the surface of the PFSA membrane (Figure 1A). STXM images and spectra of the electrochemically degraded catalyst layer show damage to the PFSA in close contact with the Pt nanoparticles (Figure 1 C and 1D). C 1s spectromicroscopy of the PFSA colocalized with the Pt film (Figure 1B) reveals that this material has a new peak at 285 eV, consistent with the formation of C═C bonds, and lower intensity associated with C−F bonds (290−310 eV). The feature at 289 eV in undamaged PFSA, which is attributed to C 1s(C═O) → π^*_{COO} transitions at carboxyl termination sites,[38] is relatively unaffected, whereas the peaks at 292.6 and 296 eV, attributed to C 1s(C−F) → $\sigma^*_{CF}(\parallel)$ and C 1s(C−F) → $\sigma^*_{CF}(\perp)$ transitions,[38] have disappeared. In addition, the signal in the pre-C 1s region (278−282 eV) is drastically reduced (especially when the pre-C 1s signal is compared to the carbon edge jump $OD_{320\ eV}-OD_{280\ eV}$), which indicates a local reduction in the fluorine concentration. Component maps (spatial distributions) of degraded PFSA, unmodified PFSA, epoxy, and Pt were derived by SVD fitting (see experimental

https://dx.doi.org/10.1021/acscatal.0c01594
ACS Catal. 2020, 10, 8285−8292

methods) and used to produce color-coded chemical maps of each species (Figure 1C). The degraded PFSA, unmodified PFSA, and Pt are colored red, green, and blue, respectively. The spatial distribution of the degraded PFSA closely tracks the Pt catalyst. Material hundreds of nanometers away from the Pt band yields spectra consistent with unmodified PFSA. The thickness of the damaged layer is on the same scale as the spot size and pixel spacing (80 nm) used when measuring the data in this figure. This coarse sampling was used to minimize dose and thus radiation damage. Image sequences (stacks) collected at the F 1s edge are consistent with loss of the C−F bonds local to the Pt catalyst (Figure 1D), but this morphology is complicated by intrusion of the embedding epoxy (Figures S5 and S6). F 1s chemical maps show modification in the fluorine chemical environment neighboring the Pt film (Figure S6) but could not be assigned. Multiple locations across the electrode were sampled and show similar results.

These results suggest that PFSA near the Pt catalyst is irreversibly degraded at potentials found inside PEM cells, likely compromising proton conduction in the nearby region and oxygen reduction on the catalyst surface. These precise phenomena have been reported by Yandrasits et al. in fully operational PEMFC membrane electrode assemblies.[39,40] They showed that holding cells at high potentials corroded the ionomer, resulting in catalyst poisoning and loss of ionic transport to the Pt surface. However, the degraded polymer was not directly visualized and could only be detected through polymer fragments found in the effluent water and bulk spectroscopy of the membrane. Moraweitz et al. recently inferred the existence of ultrathin films of modified ionomer inside aged catalyst layers using high-resolution atomic force microscopy.[41] PFSA close to catalyst particles was observed to swell less in the presence of water, and a chemical or morphological change in the PFSA was proposed. While scanning probe techniques are powerful complementary tools for characterizing the ionomer morphology, interpretation of the images is challenging and chemical speciation at the agglomerate level is not possible.

Oxidative stability testing of PFSA in full PEM cells is normally conducted using a potential hold at open circuit, approximately 0.9−1.0 V.[42] While these cathode potentials are lower than those used in this study, the damage accrues over tens to hundreds of hours. The bulk ionomer is oxidized primarily through radicals generated from H_2O_2 or from hydrogen crossover.[43] H_2O_2 is sufficiently long lived to diffuse throughout the device, damaging the bulk of the membrane.[44] Because hydrogen crossover does not occur in the half-cell geometry used here, this damage mechanism can be fully decoupled from the electrochemical treatment.

The ionomer literature has almost exclusively focused on chemical stability against peroxide and radical attack.[43,45,46] Our results suggest the reactivity of PFSA on Pt catalyst surfaces should be more carefully evaluated. The ultrathin, conformal coating of degraded electrolyte at the nanoparticle surface strikingly resembles the solid−electrolyte−interphase (SEI) layers formed inside batteries. This near-surface damage is differentiated from the less localized, radical-associated ionomer degradation which occurs throughout the bulk of the ionomer. As demonstrated in real cells,[39] oxidized ionomer at the catalyst surface creates an important barrier to ionic transport, contributing to performance loss inside the device.

The maximum cathode potential experienced in conventional PEM H_2 fuel cells is around 1.5 V vs the reversible hydrogen electrode (RHE) during transient startup/shutdown or local fuel starvation events.[47] However, many related PEM technologies including electrolyzers, microelectromechanical actuators, and reversible fuel cells routinely operate at higher oxygen-evolving potentials. To better understand the chemistry of the Pt−PFSA interface in these devices, another electrode was prepared and imaged after cycling the electrode into the initial stages of oxygen evolution. The upper potential limit was progressively incremented to a final value of 1.79 V vs RHE (Table S1, Figure S10).

STXM images and spectromicroscopy of this heavily electrochemically damaged electrode (Figure 2) show similar

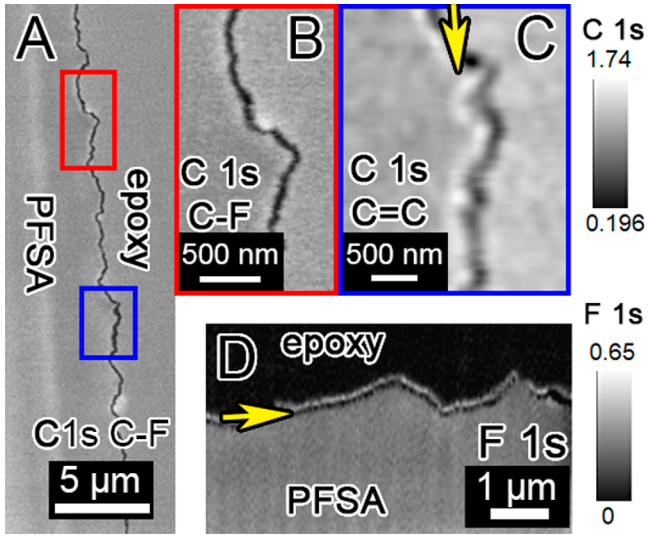

Figure 2. Single-energy STXM images of the electrode cross section after cycling to 1.79 V. Central line (black in A, B, and C, white in D) corresponds to the Pt film. Labels on each figure indicate the element and functional group being mapped. C 1s map of the PFSA C−F bonds, $OD_{292-278}$eV (A). Enlargement of A, same image (B). (C) C 1s map of C=C bonds, $OD_{284.9-280}$ eV. (D) F 1s stack map of C−F bonds, $OD_{689-680}$ eV. Yellow arrows indicate the layer of electrochemically damaged PFSA next to the Pt film; color scale indicates optical density.

but more extensive damage to the PFSA at the Pt interface. The intensity of the signal for PFSA at 292 eV immediately next to the Pt film was observed to be slightly higher than that in the bulk material (Figure 2B). This is likely caused by a distortion in the sample thickness created during ultrathin section sample preparation. High-resolution maps recorded at 285 eV show a large increase in the number of C=C bonds, as indicated by a yellow arrow (Figure 2C). The damage forms a white band (higher C=C content) that traces the Pt layer and is more pronounced than the effect observed in the sample cycled to only 1.5 V. In addition, this damage penetrates 100−150 nm into the PFSA side of the interface. Maps collected at the F 1s edge indicate a localized depletion of fluorine, as indicated by the black band, marked with a yellow arrow (Figure 2D).

The electrochemistry of the surface was investigated with cyclic voltammetry (CV) experiments. The CV curves recorded while purging the working electrode with an argon atmosphere both before and after cycling 5000 times to 1.5 V are quite similar. No redox active degradation products of the ionomer could be detected as a result of the electrochemical cycling (Figure S8). Interestingly, the apparent electrochemi-

https://dx.doi.org/10.1021/acscatal.0c01594
ACS Catal. 2020, 10, 8285−8292

cally active surface area of the catalyst layer only decreased by 10% after cycling, as determined by integrating the charge passed by hydrogen desorption (0.05−0.5 V, red and black traces). On conventional Pt/C catalysts this cycling protocol causes severe carbon corrosion, concurrent with detachment and ripening of the Pt particles, decreasing their active area. Because the electrolessly deposited Pt used here is not supported on carbon and has a relatively large initial particle size of approximately 5 nm,[32] it is mostly stable against these degradation mechanisms. Polarization curves were recorded while purging the cell with O_2 gas to measure the activity for the oxygen reduction reaction (Figure S9). The cycled catalyst layer displays significantly lower electrocatalytic performance (48% drop at 0.9 V) compared with the unaged catalyst.

The degree to which these changes in the electrocatalytic activity can be associated with the PFSA at the interface, instead of Pt degradation, is difficult to precisely determine. Our results are consistent with catalyst poisoning from PFSA degradation. Ionomer side-chain fragments produced at high potentials poison the oxygen reduction activity at even trace levels.[40] However, direct measurements of the electrocatalytic performance are not conclusive. Many factors including surface defects,[48] crystallography, and even shape[49] greatly influence the Pt specific activity and are known to be altered by cycling to high potentials, in addition to specific adsorption of poisons. This catalyst poisoning is known to be at least partially reversible, since low potentials desorb the anionic PFSA fragments, further complicating electrochemical analysis. This reversibility may offer a path toward isolating the ionomer degradation from irreversible Pt degradation in future investigations. Decoupling these concurrent degradation processes will require model systems which can precisely recreate specific aspects of the device operation.

The measurable thickness of the damaged layer hints at the mechanism of the degradation. The thickness in these images indicates that the degradation extends beyond the actual surface of the Pt itself, at least for such high potentials. Reactive species (e.g., •OOH, •OH, •H) created inside the operational cells have short lifetimes in aqueous media (10^{-6}–10^{-9} s) and cannot diffuse long distances.[50] However, a single hydroxyl radical can initiate chain reactions, generating dozens of secondary radicals, which can diffuse further.[51] The reversible potential for water oxidation to H_2O_2 on PtO_2 surfaces is 1.77 V.[52] The current efficiency for this two-electron oxidation is also low relative to four-electron oxidation to O_2. Therefore, the cycling does not generate significant amounts of peroxide directly, and this species cannot explain the polymer degradation. Alternatively, polymer chain scission occurring on the Pt surface would generate short-chain, soluble PFSA fragments.[53] Backbone scission in PFSA produces COOH-terminated strands, which are prone to sequential chain end cleavage.[54] This "unzipping" chemistry may propagate the damage away from the Pt surface, up to the length of the polymer strand.[55] The precise mechanism for the degradation remains unclear. Several different processes may contribute to the structure of the observed film.

Pt-Catalyzed Oxidation of PFSA with Peroxide. The relationship between peroxide-induced damage and direct electrochemical damage to the PFSA was further investigated by measuring catalyst layers exposed to H_2O_2 (Figure 3). Because simulating hydrogen peroxide exposure inside an operational PEMFC is challenging, simple immersion of the PFSA in solutions of H_2O_2 or Fenton's reagent is often used to evaluate the oxidative stability.[46] Here, the catalyst-coated membrane was immersed in 15 wt % aqueous H_2O_2 for 30 days. The entire membrane and catalyst layer are exposed to H_2O_2, but their decomposition toward O_2 and water occurs catalytically on the Pt surface. Radical products generated on the Pt surface would be locally concentrated. Hydrogen peroxide also electrochemically polarizes the Pt particles, even though they are not externally wired to a potentiostat. The potential established at the Pt−ionomer interface is a complex function of mass transport, concentration gradients, and multistep reaction kinetics.[56] The ionomer near the Pt surface in the presence of peroxide can be considered to experience a combined chemical and electrochemical treatment.

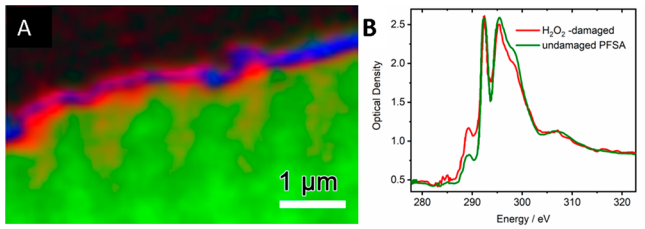

Figure 3. STXM cross section of the Pt catalyst layer damaged by hydrogen peroxide exposure. (A) Color-coded chemical map of undamaged PFSA (green), damaged PFSA (red), and Pt (blue) derived from fits to C 1s spectra. (B) C 1s X-ray absorption spectra extracted from the regions shown in A, which were used as reference spectra in the analysis.

STXM cross-section images show that the peroxide-treated and electrochemically degraded samples result in different interfacial chemistry. C 1s STXM images of the peroxide-treated catalyst layer show that the bulk PFSA membrane was not modified, but a thin film of degraded PFSA is observed (Figure 3). As before, the modified PFSA is colocalized with the Pt film at the interface, showing a thickness of 100−200 nm. However, the pre-edge C 1s spectroscopy of the peroxide and electrochemically degraded interfaces are distinct (Figure 3B). The peroxide-treated film exhibits a much stronger peak at 289 eV, with only minor changes at 284.9 eV. This is consistent with the formation of carboxylic acid moieties but not the carbon−carbon double bonds seen in the electrochemically cycled layers. The F 1s spectra of both treatments are similar and less diagnostic, showing a local decrease in the quantity of C−F bonds near the Pt surface (Figures 2D and S7). Inside real PEMFCs, direct electrochemical degradation and peroxide-induced radical damage of the PFSA could occur together, perhaps even synergistically. The ability of this model system to identify and differentiate specific degradation mechanisms is a major advantage in understanding the complex behavior of real devices.

The peroxide-treated film also serves as a negative control for carbon contamination. In order to perform the electrochemical cycling, the catalyst layers need to be pressed against carbon paper coated with carbon black. Partially graphitized carbon black would be spectroscopically similar to C=C bonds produced from degradation of PFSA and is challenging to differentiate using STXM alone. We therefore suspected that some of the features in Figures 1B and 2C could be attributed to carbon support particles adhering to the Pt−PFSA interface. Careful comparison of the C 1s spectra from carbon support particles and the electrochemically cycled catalyst layer show differences in the relative intensities of the C 1s → σ^* and C 1s → π^* transitions (Figure S12). Electron

https://dx.doi.org/10.1021/acscatal.0c01594
ACS Catal. 2020, 10, 8285−8292

microscopy of the delaminated electrode detected only trace carbon aggregates on the electrode surface after rinsing (Figures S17−S19). It seems unlikely that such contamination would form a contiguous film underneath the Pt coating with cycling-dependent thickness. Because the peroxide-treated sample was not tested electrochemically or pressed against carbon paper, no possibility of contamination exists for this sample and the observed changes can be attributed exclusively to the degradation of the PFSA at the Pt interface.

X-ray Beam Damage at the Pt−PFSA Interface. Additional control experiments were performed to ensure that the modified chemistry at the Pt/PFSA interface was not an artifact of the X-ray beam. PFSA has been shown to be extremely sensitive to electron beam[57] and X-ray damage.[58,59] The methodology used here has been optimized to minimize this damage, including low-dose collection strategies, quantitative dosimetry, and appropriate data processing.[60] These precautions allow for STXM imaging of catalyst layer samples at high spatial resolution, near the limits of current instrumentation. Particular care is necessary with composites of hard and soft matter, whose radiation sensitivity often exceeds a simple linear combination of that of the pure components. The beam sensitivity of these materials prevents detailed analysis of the Pt−ionomer interface using conventional electron microscopy techniques and likely explains why these phenomena have not been reported previously.

Pt nanoparticles were grown inside a conventional PFSA membrane. Ion exchanging the protons for $Pt(NH_3)_4^{2+}$ ions followed by reduction with gaseous H_2 produced metallic nanoparticles approximately 100 nm in diameter dispersed throughout the bulk of the PFSA (Figure S13). These Pt particles are large enough to be individually resolved with the STXM (Figure 4, left). A maximum resolution C 1s image

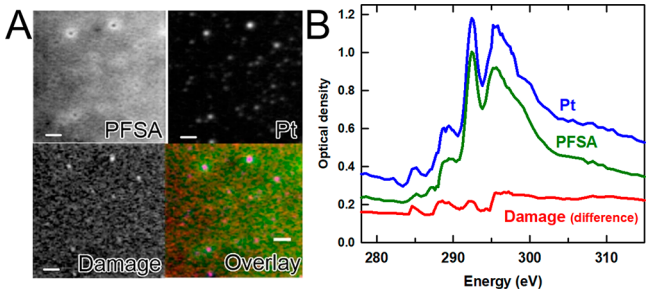

Figure 4. PFSA, damaged PFSA, and Pt maps derived from a C 1s STXM stack measured on a sample of Pt nanoparticles dispersed in a PFSA membrane. In the color composite (overlay, A), the undamaged PFSA spectrum is green and the X-ray damaged PFSA is red. Scale bars are 500 nm. (B) Extracted C 1s spectra corresponding to each mapped phase.

stack was collected, which produced substantial radiation damage (Figure S14). This damage is concentrated on the Pt nanoparticles, which are less transparent on account of their high electron density, locally increasing the X-ray absorption. This absorbed energy is transferred to the surrounding PFSA. The rigid 100 nm nanoparticles embedded in the soft PFSA causes bulging of the polymer around the particle during microtomy of nominally 50 nm ultrathin sections. This local thickening results in a white "halo" of PFSA surrounding each dark nanoparticle in Figure 4A (top left image). This morphology was confirmed by atomic force microscopy (AFM) (Figure S15).

The spectra of the X-ray-damaged PFSA contains features from both the electrochemically degraded and the peroxide-treated PFSA (Figure 4, right). It shows the formation of both C═C and C═O bonds at 284.9 and 289 eV. This is expected because radiolysis and electrochemical/radical degradation likely share intermediates and reaction products. The relative intensities of the 284.9 and 289 eV bands compared to the main C−F peaks distinguish the spectral fingerprint of beam-damaged PFSA versus electrochemical and peroxide radical damage. The locally enhanced X-ray damage from the Pt nanoparticles observed in Figure 4 does not significantly propagate into the surrounding PFSA. Low-energy photoelectrons generated by Pt atoms from X-ray absorption have mean free paths of approximately 5 nm. Fourier transform infrared (FTIR) microscopy on the irradiated PFSA containing dispersed Pt nanoparticles showed similar features to those reported previously for pure PFSA exposed to X-rays[59,61] and electron beams[62] (Figure S16). Multiple broad peaks assignable to C═C and C═O bonds (1650−1800 cm^{-1}) appear in a radiation dose-dependent fashion, consistent with the X-ray spectra. The relative intensities of these peaks change with X-ray dose, indicating the product distribution is altered as damage progresses. A fresh catalyst film not subjected to peroxide or electrochemical treatment was also measured with STXM as a negative control (Figures S20−S23). Only minimal changes in the X-ray spectroscopy were observed, and no band of degraded polymer was formed on the PFSA side of the interface. While these procedures minimize the radiation damage artifacts, they cannot be entirely eliminated and limit the obtainable spatial resolution using this model system. For ease of comparison, the C 1s spectra obtained for PFSA exposed to peroxide, electrochemical oxidation, and X-rays as well as undamaged PFSA and carbon black are overlaid in Figure S24.

The reaction mechanisms of ionomer decomposition under chemical and electrochemical degradation require further scrutiny. Ghassemzadeh et al. showed that different reactive species (i.e., •H and •OH) target different functional groups in PFSA, generating complex and unique cocktails of soluble fragments.[63,64] Some of these species could not be reliably identified, even using high-field ^{19}F NMR. In this study, the radiation damage is nonselective. X-rays above the C 1s edge excite all carbon atoms equally, leading to radical dissociation at all possible bonds. Radiation damage reflects the relative recombination rate of each carbon-centered radical created from both the initial absorption event, Auger emission, and the larger number of low-energy secondary electrons created by each X-ray. Peroxide exposure generates mixtures of •H, •OH, and •OOH radicals. These species attack the tertiary carbons and ether linkages in the main chain and side chain through broadly accepted mechanisms (Schemes S1 and S2).[46] The mechanism of electrochemical degradation could operate through direct oxidation of PFSA on the Pt surface to a radical cation, a more complex multielectron transfer, or indirectly by generating reactive radical species. No obvious mechanism for the electrochemical formation of C═C bonds has been reported for PFSA. However, in PTFE, perfluorovinyl moieties were shown to form through elimination at secondary carbon radicals (the inverse of classical radical olefin polymerization) or from radical recombination.[65] C═C bonds could also form after F cleavage from two neighboring carbon atoms, induced by electrochemical damage or irradiation.[38,59] The X-ray spectra of irradiated PFSA

https://dx.doi.org/10.1021/acscatal.0c01594
ACS Catal. 2020, 10, 8285−8292

indicating loss of F content and disruption of $-CF_2-CF_2-$ packing is also consistent with this proposed mechanism. Radicals and C=C bonds in PTFE both disappear after annealing under O_2 atmosphere,[65] indicating that these groups are transient reactive intermediates and may not persist indefinitely inside the oxidative environment of operational fuel cells. Because PEM cathode catalysts inside functional devices operate under a heated O_2 environment, a different distribution of final reaction products could be reasonably expected.

X-ray spectroscopy of electrochemically degraded PEM fuel-cell membrane electrode assemblies has been reported in a number of studies.[35,60] However, covalent modification of PFSA at the Pt interface has not been observed previously to the best of our knowledge. This is probably because most of the carbon in conventional PEMFC electrodes is in the partially graphitized carbon black support and not the ionomer phase. Graphite has an especially strong absorption feature at 285 eV associated with sp^2 carbons. These small spectral changes in the ionomer would therefore be completely masked in electronic or vibrational spectra. Unfortunately, conventional electron microscopy stains for C=C bonds, such as RuO_4, also adsorb nonspecifically to PFSA.[66] The relative paucity of analytical techniques capable of mapping and speciating nanostructured soft matter is a serious challenge in characterizing these systems.

The formation and management of SEI layers and electrolyte degradation is carefully controlled in the battery field.[67−69] This often includes chemical/potential pretreatments,[70] control over thermal[71] and voltage excursions, and use of additives. These steps are necessary because electron and ion transport across the SEI layer is critically important for maintaining the durability of functional battery devices. The local agglomerated environment and ionomer morphology inside PEM catalyst layers is critical toward establishing cell stability and performance, where the polymer electrolyte serves as both binder and proton conduction media.[30] Further work is necessary to probe the nanostructure and chemistry of the catalyst microenvironment, where delicate ultrathin ionomer coatings play a decisive role.[10,72]

CONCLUSION

In conclusion, Pt catalyst particles were shown to develop a thin coating of chemically damaged PFSA after being exposed to electrochemical oxidation. Chemical modifications at the interface of individual catalyst nanoparticles and an ionomer coating could be directly resolved. X-ray spectroscopy of this material reveals several changes in composition, including loss of C−F bonds and formation of C=C and C=O moieties. Cycling to higher potentials appeared to increase the thickness of the damaged region. Exposure of the catalyst layer to hydrogen peroxide formed a damaged ionomer film with similar morphology but different reaction products. X-ray spectra indicated the formation of carboxylic acids, instead of carbon−carbon double bonds. Radiation damage, peroxide exposure, and electrochemical oxidation result in similar chemical modifications but can be decoupled using a combination of nanoimaging and multiple spectroscopic techniques. C 1s NEXAFS in particular is well suited to differentiate these different damage mechanisms (Figure S24). Further development in nondestructive high-resolution imaging (e.g., low dose and cryomicroscopy) is necessary to better understand the evolution of these buried interfaces. While the influence of polymer electrolyte degradation at the catalyst surface has been validated in fuel-cell devices, this film has been directly visualized for the first time.

ASSOCIATED CONTENT

Supporting Information

The Supporting Information is available free of charge at https://pubs.acs.org/doi/10.1021/acscatal.0c01594.

Additional STXM images, AFM, FTIR microscopy, electron microscopy, sample preparation, and electrochemical characterization (PDF)

AUTHOR INFORMATION

Corresponding Author

Isaac Martens − *European Synchrotron Radiation Facility, Grenoble 38043, France; Department of Chemistry, University of British Columbia, Vancouver, British Columbia V6T 1Z1, Canada;* orcid.org/0000-0001-8342-6629; Email: isaac.martens@esrf.fr

Authors

Lis G. A. Melo − *Department of Chemistry & Chemical Biology, McMaster University, Hamilton, Ontario L8S 4M1, Canada;* orcid.org/0000-0001-5427-1867

Marcia M. West − *Department of Chemistry & Chemical Biology, McMaster University, Hamilton, Ontario L8S 4M1, Canada*

David P. Wilkinson − *Department of Chemical Engineering, University of British Columbia, Vancouver, British Columbia V6T 1Z1, Canada*

Dan Bizzotto − *Department of Chemistry, University of British Columbia, Vancouver, British Columbia V6T 1Z1, Canada;* orcid.org/0000-0002-2176-6799

Adam P. Hitchcock − *Department of Chemistry & Chemical Biology, McMaster University, Hamilton, Ontario L8S 4M1, Canada;* orcid.org/0000-0002-1598-7886

Complete contact information is available at: https://pubs.acs.org/10.1021/acscatal.0c01594

Notes

The authors declare no competing financial interest.

ACKNOWLEDGMENTS

This work was financially supported by the Natural Sciences and Engineering Council of Canada (NSERC) and the Automotive Partnership of Canada through the Catalyst Research for Polymer Electrolyte Fuel Cells (CaRPE-FC) program. I.M. acknowledges scholarship support from NSERC. We thank Gethin Owen and the UBC Centre for High Throughput Genomics at UBC for providing electron microscopy support. Research described in this paper was performed using the ambient-STXM on beamline 10ID1 at the Canadian Light Source, which is supported by the Canadian Foundation for Innovation (CFI), and at beamline 5.3.2.2 at the Advanced Light Source, which is supported by the Director of the Office of Science, Department of Energy, under Contract No. DE-AC02-05CH11231. We thank staff scientists Jian Wang at CLS and David Kilcoyne at ALS for their assistance and support of the beamlines and STXMs. A. Korinek and G. Botton are gratefully acknowledged for providing the TEM image, carried out at the Canadian Centre

for Electron Microscopy, supported by NSERC, CFI, and McMaster University.

REFERENCES

(1) Dubau, L.; Castanheira, L.; Maillard, F.; Chatenet, M.; Lottin, O.; Maranzana, G.; Dillet, J.; Lamibrac, A.; Perrin, J.-C.; Moukheiber, E.; ElKaddouri, A.; De Moor, G.; Bas, C.; Flandin, L.; Caqué, N. A Review of PEM Fuel Cell Durability: Materials Degradation, Local Heterogeneities of Aging and Possible Mitigation Strategies. *Wiley Interdiscip. Rev. Energy Environ.* **2014**, *3*, 540−560.
(2) Banham, D.; Ye, S.; Pei, K.; Ozaki, J.; Kishimoto, T.; Imashiro, Y. A Review of the Stability and Durability of Non-Precious Metal Catalysts for the Oxygen Reduction Reaction in Proton Exchange Membrane Fuel Cells. *J. Power Sources* **2015**, *285*, 334−348.
(3) Sui, S.; Wang, X.; Zhou, X.; Su, Y.; Riffat, S.; Liu, C.-j. A Comprehensive Review of Pt Electrocatalysts for the Oxygen Reduction Reaction: Nanostructure, Activity, Mechanism and Carbon Support in PEM Fuel Cells. *J. Mater. Chem. A* **2017**, *5*, 1808−1825.
(4) Soboleva, T.; Zhao, X.; Malek, K.; Xie, Z.; Navessin, T.; Holdcroft, S. On the Micro-, Meso-, and Macroporous Structures of Polymer Electrolyte Membrane Fuel Cell Catalyst Layers. *ACS Appl. Mater. Interfaces* **2010**, *2*, 375−384.
(5) Shojaeefard, M. H.; Molaeimanesh, G. R.; Nazemian, M.; Moqaddari, M. R. A Review on Microstructure Reconstruction of PEM Fuel Cells Porous Electrodes for Pore Scale Simulation. *Int. J. Hydrogen Energy* **2016**, *41*, 20276−20293.
(6) Venkatesan, S. V.; Lim, C.; Holdcroft, S.; Kjeang, E. Progression in the Morphology of Fuel Cell Membranes upon Conjoint Chemical and Mechanical Degradation. *J. Electrochem. Soc.* **2016**, *163*, F637−F643.
(7) Kneer, A.; Jankovic, J.; Susac, D.; Putz, A.; Wagner, N.; Sabharwal, M.; Secanell, M. Correlation of Changes in Electrochemical and Structural Parameters Due to Voltage Cycling Induced Degradation in PEM Fuel Cells. *J. Electrochem. Soc.* **2018**, *165*, F3241−F3250.
(8) Inaba, M.; Yamada, H.; Tokunaga, J.; Tasaka, A. Effect of Agglomeration of Pt/C Catalyst on Hydrogen Peroxide Formation. *Electrochem. Solid-State Lett.* **2004**, *7*, A474.
(9) White, R. T.; Ramani, D.; Eberhardt, S.; Najm, M.; Orfino, F. P.; Dutta, M.; Kjeang, E. Correlative X-Ray Tomographic Imaging of Catalyst Layer Degradation in Fuel Cells. *J. Electrochem. Soc.* **2019**, *166*, F914−F925.
(10) Zhang, S.; Yuan, X. Z.; Hin, J. N. C.; Wang, H.; Friedrich, K. A.; Schulze, M. A Review of Platinum-Based Catalyst Layer Degradation in Proton Exchange Membrane Fuel Cells. *J. Power Sources* **2009**, *194*, 588−600.
(11) Trotsenko, O.; Koestner, R.; Roiter, Y.; Tokarev, A.; Minko, S. Probing Rough Composite Surfaces with Atomic Force Microscopy: Nafion Ionomer in Fuel Cell Electrodes. *Polymer* **2016**, *102*, 396−403.
(12) Koestner, R. J.; Cullen, D. A.; Kukreja, R.; Minko, S.; Meyer, H. M.; Liu, Z.; More, K. L. High-Resolution Mapping of the PFSA Polymer Distribution in PEFC Electrode Layers. *ECS Trans.* **2014**, *64*, 819−827.
(13) Allen, F. I.; Comolli, L. R.; Kusoglu, A.; Modestino, M. A.; Minor, A. M.; Weber, A. Z. Morphology of Hydrated As-Cast Nafion Revealed through Cryo Electron Tomography. *ACS Macro Lett.* **2015**, *4*, 1−5.
(14) Sabharwal, M.; Pant, L. M.; Putz, A.; Susac, D.; Jankovic, J.; Secanell, M. Analysis of Catalyst Layer Microstructures: From Imaging to Performance. *Fuel Cells* **2016**, *16*, 734−753.
(15) Yakovlev, S.; Balsara, N. P.; Downing, K. H. Insights on the Study of Nafion Nanoscale Morphology by Transmission Electron Microscopy. *Membranes (Basel, Switz.)* **2013**, *3*, 424−439.
(16) Holdcroft, S. Fuel Cell Catalyst Layers: A Polymer Science Perspective. *Chem. Mater.* **2014**, *26*, 381−393.
(17) Karan, K. PEFC Catalyst Layer: Recent Advances in Materials, Microstructural Characterization, and Modeling. *Curr. Opin. Electrochem.* **2017**, *5*, 27−35.
(18) Garrick, T. R.; Moylan, T. E.; Yarlagadda, V.; Kongkanand, A. Characterizing Electrolyte and Platinum Interface in PEM Fuel Cells Using CO Displacement. *J. Electrochem. Soc.* **2017**, *164*, F60−F64.
(19) Shinozaki, K.; Pivovar, B. S.; Kocha, S. S. Enhanced Oxygen Reduction Activity on Pt/C for Nafion-Free, Thin, Uniform Films in Rotating Disk Electrode Studies. *ECS Trans.* **2013**, *58*, 15−26.
(20) Xie, J.; Garzon, F.; Zawodzinski, T.; Smith, W. Ionomer Segregation in Composite MEAs and Its Effect on Polymer Electrolyte Fuel Cell Performance. *J. Electrochem. Soc.* **2004**, *151*, A1084.
(21) Subbaraman, R.; Strmcnik, D.; Stamenkovic, V.; Markovic, N. M. Three Phase Interfaces at Electrified Metal-Solid Electrolyte Systems 1. Study of the Pt(Hkl)-Nafion Interface. *J. Phys. Chem. C* **2010**, *114*, 8414−8422.
(22) Gómez-Marín, A. M.; Berná, A.; Feliu, J. M. Spectroelectrochemical Studies of the Pt(111)/Nafion Interface Cast Electrode. *J. Phys. Chem. C* **2010**, *114*, 20130−20140.
(23) Zeng, J.; Jean, D.; Ji, C.; Zou, S. In Situ Surface-Enhanced Raman Spectroscopic Studies of Nafion Adsorption on Au and Pt Electrodes. *Langmuir* **2012**, *28*, 957−964.
(24) Malevich, D.; Li, J.; Chung, M. K.; McLaughlin, C.; Schlaf, M.; Lipkowski, J. In Situ IR Reflectance Absorption Spectroscopy Studies of the Effect of Nafion on CO Adsorption and Electrooxidation at Pt Nanoparticles. *J. Solid State Electrochem.* **2005**, *9*, 267−276.
(25) Hanawa, H.; Kunimatsu, K.; Watanabe, M.; Uchida, H. In Situ ATR-FTIR Analysis of the Structure of Nafion Pt/C and Nafion Pt 3 Co/C Interfaces in Fuel Cell. *J. Phys. Chem. C* **2012**, *116*, 21401−21406.
(26) Yagi, I.; Inokuma, K.; Kimijima, K.; Notsu, H. Molecular Structure of Buried Perfluorosulfonated Ionomer/Pt Interface Probed by Vibrational Sum Frequency Generation Spectroscopy. *J. Phys. Chem. C* **2014**, *118*, 26182−26190.
(27) Masuda, T.; Sonsudin, F.; Singh, P. R.; Naohara, H.; Uosaki, K. Potential-Dependent Adsorption and Desorption of Perfluorosulfonated Ionomer on a Platinum Electrode Surface Probed by Electrochemical Quartz Crystal Microbalance and Atomic Force Microscopy. *J. Phys. Chem. C* **2013**, *117*, 15704−15709.
(28) Wood, D. L.; Chlistunoff, J.; Majewski, J.; Borup, R. L. Nafion Structural Phenomena at Platinum and Carbon Interfaces. *J. Am. Chem. Soc.* **2009**, *131*, 18096−18104.
(29) Sleightholme, A. E. S. S.; Kucernak, A. An Anomalous Peak Observed in the Electrochemistry of the Platinum/Perfluorosulfonic Acid Membrane Interface. *Electrochim. Acta* **2011**, *56*, 4396−4402.
(30) Kongkanand, A.; Mathias, M. F. The Priority and Challenge of High-Power Performance of Low-Platinum Proton-Exchange Membrane Fuel Cells. *J. Phys. Chem. Lett.* **2016**, *7*, 1127−1137.
(31) Ohma, A.; Yamamoto, S.; Shinohara, K. Membrane Degradation Mechanism during Open-Circuit Voltage Hold Test. *J. Power Sources* **2008**, *182*, 39−47.
(32) Martens, I.; Pinaud, B. A.; Baxter, L.; Wilkinson, D. P.; Bizzotto, D. Controlling Nanoparticle Interconnectivity in Thin-Film Platinum Catalyst Layers. *J. Phys. Chem. C* **2016**, *120*, 21364−21372.
(33) Blom, D. A.; Dunlap, J. R.; Nolan, T. A.; Allard, L. F. Preparation of Cross-Sectional Samples of Proton Exchange Membrane Fuel Cells by Ultramicrotomy for TEM. *J. Electrochem. Soc.* **2003**, *150*, A414.
(34) Ingle, N. J. C. J. C.; Sode, A.; Martens, I.; Gyenge, E.; Wilkinson, D. P. P.; Bizzotto, D. Synthesis and Characterization of Diverse Pt Nanostructures in Nafion. *Langmuir* **2014**, *30*, 1871−1879.
(35) Hitchcock, A. P.; Berejnov, V.; Lee, V.; West, M.; Colbow, V.; Dutta, M.; Wessel, S. Carbon Corrosion of Proton Exchange Membrane Fuel Cell Catalyst Layers Studied by Scanning Transmission X-Ray Microscopy. *J. Power Sources* **2014**, *266*, 66−78.
(36) *Fuel Cell Technical Team Roadmap*; U.S. DRIVE Partnership/Fuel Cell Technical Team: Washington, DC, 2013.
(37) Hitchcock, A. P. Soft X-Ray Imaging and Spectromicroscopy. In *Handbook of Nanoscopy*; Tendeloo Van, G., Dyck, V. D., Pennycook, S. J., Eds.; Wiley-VCH Verlag GmbH & Co. KGaA: Weinheim, Germany, 2012; pp 745−791.

https://dx.doi.org/10.1021/acscatal.0c01594
ACS Catal. 2020, 10, 8285−8292

(38) Yan, Z. B.; Hayes, R.; Melo, L. G. A.; Goward, G. R.; Hitchcock, A. P. X-Ray Absorption and Solid-State NMR Spectroscopy of Fluorinated Proton Conducting Polymers. *J. Phys. Chem. C* **2018**, *122*, 3233−3244.
(39) Yandrasits, M.; Lindell, M.; Komlev, A.; Fort, E.; Hamrock, S.; Peppin, D. M.; Kalstabakken, K. Stability of Perfluoro Bis(Sulfonyl)-Imide-Based Ionomers in Fuel Cell Membranes and Electrodes. *ECS Trans.* **2018**, *86*, 381−394.
(40) Yandrasits, M.; Lindell, M.; Peppin, D.; Komlev, A.; Hamrock, S.; Haugen, G.; Fort, E.; Kalstabakken, K. Chemical Stability of Perfluorobis(Sulfonyl)Imide-Acid (PFIA) Ionomers in Open Circuit Voltage (OCV) Accelerated Test Conditions. *J. Electrochem. Soc.* **2018**, *165*, F3261−F3270.
(41) Morawietz, T.; Handl, M.; Oldani, C.; Gazdzicki, P.; Hunger, J.; Wilhelm, F.; Blake, J.; Friedrich, K. A.; Hiesgen, R. High-Resolution Analysis of Ionomer Loss in Catalytic Layers after Operation. *J. Electrochem. Soc.* **2018**, *165*, F3139−F3147.
(42) *Fuel Cell Technologies Office Multi-Year Research, Development and Demonstration Plan - 3.4 Technical Plan - Fuel Cells*; U.S. Department of Energy, 2012.
(43) Kusoglu, A.; Weber, A. Z. New Insights into Perfluorinated Sulfonic-Acid Ionomers. *Chem. Rev.* **2017**, *117*, 987−1104.
(44) Böhm, T.; Moroni, R.; Breitwieser, M.; Thiele, S.; Vierrath, S. Spatially Resolved Quantification of Ionomer Degradation in Fuel Cells by Confocal Raman Microscopy. *J. Electrochem. Soc.* **2019**, *166*, F3044−F3051.
(45) Rodgers, M. P.; Bonville, L. J.; Kunz, H. R.; Slattery, D. K.; Fenton, J. M. Fuel Cell Perfluorinated Sulfonic Acid Membrane Degradation Correlating Accelerated Stress Testing and Lifetime. *Chem. Rev.* **2012**, *112*, 6075−6103.
(46) Zatoń, M.; Rozière, J.; Jones, D. J. Current Understanding of Chemical Degradation Mechanisms of Perfluorosulfonic Acid Membranes and Their Mitigation Strategies: A Review. *Sustain. Energy Fuels* **2017**, *1*, 409−438.
(47) Cherevko, S.; Kulyk, N.; Mayrhofer, K. J. J. Durability of Platinum-Based Fuel Cell Electrocatalysts: Dissolution of Bulk and Nanoscale Platinum. *Nano Energy* **2016**, *29*, 275−298.
(48) Dubau, L.; Nelayah, J.; Moldovan, S.; Ersen, O.; Bordet, P.; Drnec, J.; Asset, T.; Chattot, R.; Maillard, F. Defects Do Catalysis: CO Monolayer Oxidation and Oxygen Reduction Reaction on Hollow PtNi/C Nanoparticles. *ACS Catal.* **2016**, *6*, 4673−4684.
(49) Chlistunoff, J.; Pivovar, B. Effects of Ionomer Morphology on Oxygen Reduction on Pt. *J. Electrochem. Soc.* **2015**, *162*, F890−F900.
(50) Gubler, L.; Dockheer, S. M.; Koppenol, W. H. Radical (HO●, H● and HOO●) Formation and Ionomer Degradation in Polymer Electrolyte Fuel Cells. *J. Electrochem. Soc.* **2011**, *158*, B755.
(51) Tomanová, K.; Precek, M.; Múčka, V.; Vyšín, L.; Juha, L.; Čuba, V. At the Crossroad of Photochemistry and Radiation Chemistry: Formation of Hydroxyl Radicals in Diluted Aqueous Solutions Exposed to Ultraviolet Radiation. *Phys. Chem. Chem. Phys.* **2017**, *19*, 29402−29408.
(52) Kozawa, A. Effects of Anions and Cations on Oxygen Reduction and Oxygen Evolution Reactions on Platinum Electrodes. *J. Electroanal. Chem.* **1964**, *8*, 20−39.
(53) Healy, J.; Hayden, C.; Xie, T.; Olson, K.; Waldo, R.; Brundage, M.; Gasteiger, H.; Abbott, J. Aspects of the Chemical Degradation of PFSA Ionomers Used in PEM Fuel Cells. *Fuel Cells* **2005**, *5*, 302−308.
(54) Borup, R.; Meyers, J.; Pivovar, B.; Kim, Y. S.; Mukundan, R.; Garland, N.; Myers, D.; Wilson, M.; Garzon, F.; Wood, D.; Zelenay, P.; More, K.; Stroh, K.; Zawodzinski, T.; Boncella, J.; McGrath, J. E.; Inaba, M.; Miyatake, K.; Hori, M.; Ota, K.; Ogumi, Z.; Miyata, S.; Nishikata, A.; Siroma, Z.; Uchimoto, Y.; Yasuda, K.; Kimijima, K.; Iwashita, N. Scientific Aspects of Polymer Electrolyte Fuel Cell Durability and Degradation. *Chem. Rev.* **2007**, *107*, 3904−3951.
(55) Hommura, S.; Kawahara, K.; Shimohira, T.; Teraoka, Y. Development of a Method for Clarifying the Perfluorosulfonated Membrane Degradation Mechanism in a Fuel Cell Environment. *J. Electrochem. Soc.* **2008**, *155*, A29.
(56) Katsounaros, I.; Schneider, W. B.; Meier, J. C.; Benedikt, U.; Biedermann, P. U.; Auer, A. A.; Mayrhofer, K. J. J. Hydrogen Peroxide Electrochemistry on Platinum: Towards Understanding the Oxygen Reduction Reaction Mechanism. *Phys. Chem. Chem. Phys.* **2012**, *14*, 7384.
(57) Cullen, D. A.; Sneed, B. T.; More, K. L. Overcoming the Challenges of Beam-Sensitivity in Fuel Cell Electrodes. *Microsc. Microanal.* **2017**, *23*, 2222−2223.
(58) Melo, L. G. A.; Hitchcock, A. P. Optimizing Soft X-Ray Spectromicroscopy for Fuel Cell Studies: X-Ray Damage of Ionomer. *Microsc. Microanal.* **2018**, *24*, 460−461.
(59) Martens, I.; Melo, L. G. A.; Wilkinson, D. P.; Bizzotto, D.; Hitchcock, A. P. Characterization of X-Ray Damage to Perfluorosulfonic Acid Using Correlative Microscopy. *J. Phys. Chem. C* **2019**, *123*, 16023−16033.
(60) Melo, L. G. A.; Hitchcock, A. P.; Jankovic, J.; Stumper, J.; Susac, D.; Berejnov, V. Quantitative Mapping of Ionomer in Catalyst Layers by Electron and X-Ray Spectromicroscopy. *ECS Trans.* **2017**, *80*, 275−282.
(61) Almeida, S. H.; Kawano, Y. Effects of X-Ray Radiation on Nafion Membrane. *Polym. Degrad. Stab.* **1998**, *62*, 291−297.
(62) Kreitmeier, S.; Michiardi, M.; Wokaun, A.; Büchi, F. N. Factors Determining the Gas Crossover through Pinholes in Polymer Electrolyte Fuel Cell Membranes. *Electrochim. Acta* **2012**, *80*, 240−247.
(63) Ghassemzadeh, L.; Kreuer, K. D.; Maier, J.; Müller, K. Chemical Degradation of Nafion Membranes under Mimic Fuel Cell Conditions as Investigated by Solid-State NMR Spectroscopy. *J. Phys. Chem. C* **2010**, *114*, 14635−14645.
(64) Ghassemzadeh, L.; Peckham, T. J.; Weissbach, T.; Luo, X.; Holdcroft, S. Selective Formation of Hydrogen and Hydroxyl Radicals by Electron Beam Irradiation and Their Reactivity with Perfluorosulfonated Acid Ionomer. *J. Am. Chem. Soc.* **2013**, *135*, 15923−15932.
(65) Fisher, W. K.; Corelli, J. C. Effect of Ionizing Radiation on the Chemical Composition, Crystalline Content and Structure, and Flow Properties of Polytetrafluoroethylene. *J. Polym. Sci., Polym. Chem. Ed.* **1981**, *19*, 2465−2493.
(66) Xue, T.; Trent, J. S.; Osseo-Asare, K. Characterization of Nafion® Membranes by Transmission Electron Microscopy. *J. Membr. Sci.* **1989**, *45*, 261−271.
(67) Wang, A.; Kadam, S.; Li, H.; Shi, S.; Qi, Y. Review on Modeling of the Anode Solid Electrolyte Interphase (SEI) for Lithium-Ion Batteries. *npj Comput. Mater.* **2018**, *4*, 15.
(68) Peled, E.; Menkin, S. Review—SEI: Past, Present and Future. *J. Electrochem. Soc.* **2017**, *164*, A1703−A1719.
(69) Xu, K. Electrolytes and Interphases in Li-Ion Batteries and Beyond. *Chem. Rev.* **2014**, *114*, 11503−11618.
(70) Holtstiege, F.; Bärmann, P.; Nölle, R.; Winter, M.; Placke, T. Pre-Lithiation Strategies for Rechargeable Energy Storage Technologies: Concepts, Promises and Challenges. *Batteries* **2018**, *4*, 4.
(71) Dubarry, M.; Truchot, C.; Liaw, B. Y.; Gering, K.; Sazhin, S.; Jamison, D.; Michelbacher, C. Evaluation of Commercial Lithium-Ion Cells Based on Composite Positive Electrode for Plug-In Hybrid Electric Vehicle Applications. *J. Electrochem. Soc.* **2013**, *160*, A191−A199.
(72) Awatani, T.; Midorikawa, H.; Kojima, N.; Ye, J.; Marcott, C. Morphology of Water Transport Channels and Hydrophobic Clusters in Nafion from High Spatial Resolution AFM-IR Spectroscopy and Imaging. *Electrochem. Commun.* **2013**, *30*, 5−8.

https://dx.doi.org/10.1021/acscatal.0c01594
ACS Catal. 2020, 10, 8285−8292